Stochastic Single-Shot Polarization Pinning of Polariton Condensate at High Temperatures

Y. C. Balas ●,[1,2,3,4,*] E. S. Sedov ●,[1,2,5] G. G. Paschos ●,[1,2] Z. Hatzopoulos,[3] H. Ohadi ●,[6]
A. V. Kavokin ●,[1,2,7,8] and P. G. Savvidis[1,2,3,4,9,†]

[1]*Foundation for Research and Technology-Hellas, Institute of Electronic Structure and Laser,*
P.O. Box 1527, 71110 Heraklion, Crete, Greece
[2]*Department of Materials Science and Technology, University of Crete, P.O. Box 2208, 71003 Heraklion, Crete, Greece*
[3]*Key Laboratory for Quantum Materials of Zhejiang Province, School of Science, Westlake University,*
18 Shilongshan Rd, Hangzhou 310024, Zhejiang, China
[4]*Westlake Institute for Advanced Study, 18 Shilongshan Rd, Hangzhou 310024, Zhejiang, China*
[5]*Vladimir State University named after A. G. and N. G. Stoletovs, Gorky str. 87, Vladimir 600000, Russia*
[6]*SUPA, University of St. Andrews, St. Andrews KY16 9SS, United Kingdom*
[7]*St. Petersburg State University, Spin Optics Laboratory, Ul'anovskaya 1, Peterhof, St. Petersburg 198504, Russia*
[8]*NTI Center for Quantum Communications, National University of Science and Technology MISiS, Moscow 119049, Russia*
[9]*Department of Nanophotonics and Metamaterials, ITMO University, 197101 St. Petersburg, Russia*

We resolve single-shot polariton condensate polarization dynamics, revealing a high degree of circular polarization persistent up to $T = 170$ K. The statistical analysis of pulse-to-pulse polariton condensate polarization elucidates the stochastic nature of the polarization pinning process, which is strongly dependent on the pump laser intensity and polarization. Our experiments show that by spatial trapping and isolating condensates from their noisy environment it is possible to form strongly spin-polarized polariton condensates at high temperatures, offering a promising route to the realization of polariton spin lattices for quantum simulations.

Many-body spin systems can model and probe complex problems such as neural networks [1], optimization problems [2], protein folding [3] and economics [4] by mapping them to experimentally controllable Hamiltonians. In addition they provide insight into collective spin behaviors with frustrated spin interactions [5]. The equilibrium realizations vary from ultracold atoms [6] to photons [7] and superconducting junctions [8]. Recently, driven-dissipative systems such as degenerate optical parametric oscillators [9] and exciton-polariton condensates [10–14] have also gained considerable interest due to their non-equilibrium nature. Exciton-polaritons (polaritons) are quasiparticles formed by the strong coupling of photons confined in dielectric microcavities to excitons confined in semiconductor quantum wells [15]. Optical selection rules establish an unambiguous connection between the polarization of photons (circular σ_+ and σ_-) and the projection of an exciton spin on the microcavity growth direction ($+1$ and -1, respectively) forming a spin-polarized polariton state. Therefore, the polarization of the emitted photoluminescence (PL) provides direct access to the spin state of a polariton condensate. Earlier works have reported peculiar observations of spin polarized polariton condensate emission attributed to an interplay between the two orthogonal linear polarizations splitting and their respective

decay rates giving rise to stable solutions described by strong circular polarization [12,13]. The onset of the bifurcation regime where the system randomly chooses between two polarization states, occurs within a narrow excitation power range with the degree of spin polarization maximized for small linear polarization splittings [16]. Thereby, strong spin polarization of the condensate is favored in the trapped geometry with suppressed energy blueshifts and unperturbed by reservoir noise.

Of particular relevance to the present work, polariton condensates have been shown to exhibit a bistable macroscopic spin at $T = 4$ K under continuous-wave (cw) excitation [12], with tunable interaction [13] in optical lattices [14]. Finding the ground state of polariton spin lattices requires multiple realizations [17], which under cw operation is too slow for dynamical studies and counteracts the potential capacity of the hundreds of Gbps computational speedup of this system. Moreover, all previous demonstrations were performed at 4 K, which hinders the practicality of this system as a physical simulator. Previous studies were suggesting that single-mode laser excitations and cryogenic temperatures are crucial for the observation of highly polarized condensates [12]. This was understood as the condensate spin stability could be critically destabilized by the noise originating from the

117401-1

pump intensity fluctuations or the reservoir temperature. In this context, ultrashort pulsed excitation with its highly nonlinear intensity and near room temperature operation was perceived to be severely inhibiting the observation of highly polarized polariton condensates.

Here, we show that optically trapped condensates in a high quality microcavity with correctly designed detuning can show single-shot circular polarization up to $T = 170$ K under ultrashort pulsed excitation. This allows for up to 75 million realizations per second enabling a detailed statistical analysis. Equipped with this capability, we study the degree of circular polarization of the condensate emission (spin) as we change the pump's polarization from circular to linear polarization at various temperatures. At low temperatures, we observe that when the laser is linearly polarized the polariton cloud randomly condenses in each pulse into either a spin-up (highly σ_+ polarized) or spin-down (highly σ_- polarized) state due to spontaneous symmetry breaking at the onset of condensation. A statistical analysis of the polarization of consecutive realizations evidences that in the linearly polarized pumping case the condensate circular polarization is spontaneous. However, if the pump is circularly polarized, this randomness is explicitly broken and the condensate forms in the same polarization state as that of the pump. As we increase the temperature from 4 to 170 K the spread of the condensate polarization distribution broadens due to the noise generated by the high temperature reservoir excitons. In the case where the pump is circularly polarized this results in a slightly broadened distribution for the circular polarization. In the linearly polarized excitation case, however, the two individually distinct polarization distributions gradually merge as temperature increases until $T = 150$ K where we observe a single distribution centered around zero.

We study the spin polarization of optically trapped polariton condensates formed in an ultrahigh finesse ($Q \approx 31000$ corresponding to a polariton lifetime of $\tau_p \approx 100$ ps) $5\lambda/2$ microcavity. Four sets of three 12-nm GaAs quantum wells are positioned at the antinodes of the $Al_{0.3}Ga_{0.7}As$ cavity. The top (bottom) Bragg mirror is composed of 45 (50) $AlAs/Al_{0.15}Ga_{0.85}As$ layers. The sample is cooled to 10 K inside a cold-finger cryostat, and exhibits a Rabi splitting of 9.2 meV [18]. The studied sample allows measurements at elevated temperatures of up to 170 K. This is facilitated by the wide range of negative detunings (28 meV) available in this sample, which compensates for the redshift of exciton energy with temperature. The condensate is excited by a nonresonant pulsed Ti:sapphire laser tuned to the reflectivity dip at the edge of the microcavity mirror stop band. Optical traps for condensates are created by the spatial patterning of the laser beam using a high-definition digital micromirror device (DMD). Furthermore, the DMD device allows fast and repeatable power dependence measurements using variable spatial dithering of the excitation pattern. [Fig. 1(a)].
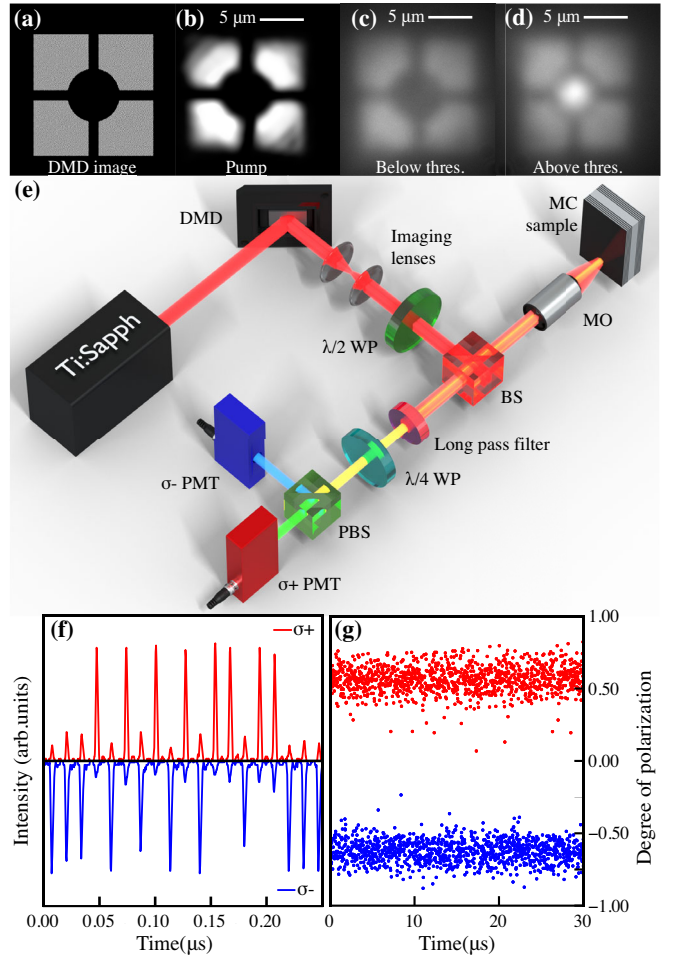

FIG. 1. (a) Pattern on the DMD, (b) spatial profile of the patterned pump beam, (c) PL below the condensation threshold, and (d) optically trapped polariton condensate near threshold. (e) Schematic of the experimental setup. (f) PL intensity time series of σ_+ and σ_- components and (g) the degree of circular polarization for each condensate realization with a linearly polarized pump.

The spatially patterned pump beam [Fig. 1(b)] is projected onto the sample using a microscope objective (MO). The pump creates a spatially distributed exciton reservoir imprinting a potential energy landscape that depends on the local pump intensity [Fig. 1(c)] [19–22]. Following the pump pulse excitation (150 fs, 75 MHz repetition rate) a polariton condensate forms with a characteristic buildup time of approximately 50 ps, which lasts for an additional 100 ps [23]. The pump can be either circularly polarized using a quarter wave plate (WP), or linearly polarized in arbitrary directions using a half WP. When the pump is linearly polarized, the polarization axis is aligned with the (100) crystallographic axis of the sample to minimize the polarization ellipticity due to sample birefringence. A standard polarimetry technique [Fig. 1(e)] is used to analyze the circular polarization of the condensate emission.
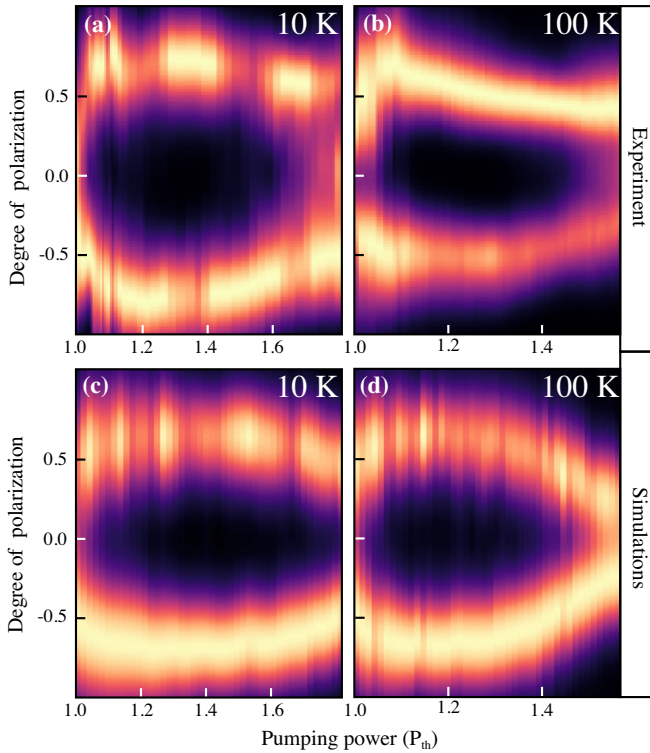
FIG. 2. Probability density function of condensate circular polarization as a function of pump power at $T = 10$ (left) and $T = 100$ K (right) in experiment (top) and theory (bottom). The pump is linearly polarized.

FIG. 3. Distribution of the degree of circular polarization s_z as a function of temperature at different pump polarizations in experiment (top) and theory (bottom). All of the experimental parameters were a subject to optimization. The pump power is $P \approx 1.2 P_{th}$ and the diameter of the trap is 4 μm for all temperatures. The detuning range is from -20 meV at 10 K to -8 meV at 170 K.

The PL is spectrally filtered from the pump scatter using a long-pass filter [Fig. 1(d)]. The circular σ_+ and σ_- components are separated using a quarter WP and a polarizing beam splitter (PBS). Each component is then detected by a photomultiplier tube (PMT). The fast PMTs (rise time ≈ 0.5 ns) together with a fast oscilloscope allow time resolving the pulse-to-pulse condensate intensity. The degree of circular polarization is $s_z = (I_{\sigma+} - I_{\sigma+})/(I_{\sigma+} + I_{\sigma-})$, where $I_{\sigma\pm}$ are the peak intensities of the corresponding polarization components. We measure s_z for each individual pulse for 100 μs at different temperatures ($T = 10$ to 170 K).

With a linearly polarized pump ($T = 10$ K), the condensate acquires a well-defined polarization in each pulse. The polarization is either predominantly right-circular σ_+ or left-circular σ_-, and can flip from one to another randomly in each realization [see pulse train in Fig. 1(f)]. A time series of the pulse train comprising 2400 realizations clearly shows the bistable behavior of the condensate spin [Fig. 1(g)]. This is in contrast to below condensation threshold, where the polarization of the PL follows the polarization of the excitation [24].

The pump power dependence of the circular polarization shows a clear bifurcation of the spin immediately above threshold [Fig. 2(a)]. With increasing pump power the two distinct distributions move closer to each other indicating reduced spin polarization, and eventually merge.
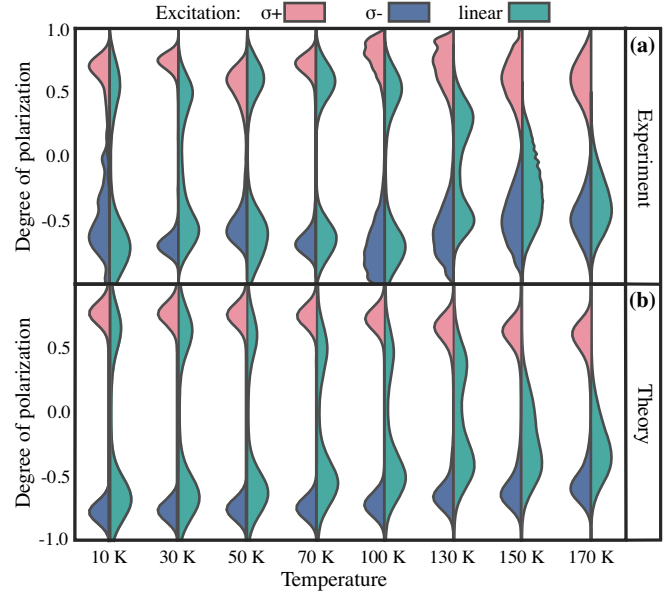
This behavior is observed for the entire temperature range (up to $T = 130$ K) [Fig. 2(b)].

A temperature scan at pump power $P \approx 1.2 P_{th}$ shows the collapse of the spin bifurcation for the linearly polarized pump case at $T = 150$ K (Fig. 3). The circular polarization probability distribution for the σ_- has a slightly higher peak. This imbalance is attributed to a slight ellipticity of the pump polarization, which induces a small symmetry breaking. With a further increase in temperature, the induced symmetry breaking starts dominating, and the condensates are formed in a uniform distribution but with a preferable circular polarization imposed by the degree of the pump polarization ellipticity.

The role of pump polarization in breaking of the polarization symmetry becomes clearer when the pump is fully circularly polarized. For the circularly polarized excitation, we observe the strong polarization (75% at 10 and 50% at 170 K) of the condensates following the polarization of the pump laser throughout the whole temperature scan.

The spontaneity of the polarization pinning is manifested in a random flipping between the two σ_+ and σ_- polarizations in sequential realizations. Here, for a sequence of realizations in the bistable system, to occur randomly (like sequential coin tosses), the realizations must be independent of each other. We examine the polarization behavior of the condensates under the linearly polarized pulse-to-pulse pumping at $T = 130$ K. We extract the probability of occurrence of n consecutive realizations of the condensates with no spin flips ($|\uparrow_1\uparrow_2 \cdots \uparrow_n\rangle$ or $|\downarrow_1\downarrow_2 \cdots \downarrow_n\rangle$) for σ_+
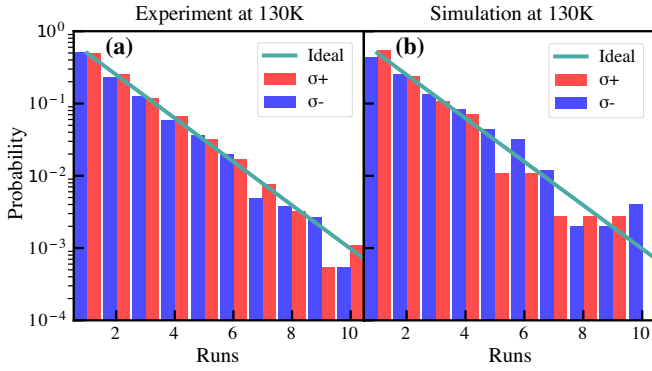
FIG. 4. The probability of the number of consecutive realizations of polariton condensates with the same polarization (Runs) under a train of linearly polarized pump pulses.

and σ_- states (see Fig. 4). The green line corresponds to the ideal case of true independence between events, which agrees remarkably well with the experiment. This evidences the spontaneity of the polarization at high temperatures, and shows that there is no transfer of spin from one realization to the next.

Theory.— The origin of the spontaneous symmetry breaking giving rise to spin bifurcation is the splitting in energy $\hbar\Delta$ and dissipation rates γ of linearly polarized polariton eigenstates. This mechanism has been discussed in relation to the experiments done with continuous wave nonresonant excitation [12–14]. It can be applied equally well in the pulsed excitation regime considered here. In addition, here we explicitly take into account the effect of temperature on the polariton polarization behavior. We simulate the evolution of the spinor order parameter $|\psi\rangle = [\psi_+(t), \psi_-(t)]^T$, where $\psi_\pm(t)$ are the amplitudes of the circular polarization components of the polariton condensate. The spinor $|\psi\rangle$ obeys the Langevin equation,

$$id_t|\psi\rangle = \frac{1}{2}[(i\gamma - \Delta)\hat{\sigma}_x + \hat{V} + i(\hat{R} - \Gamma\hat{\sigma}_0)]|\psi\rangle + \hat{D}|\eta\rangle. \quad (1)$$

The operator $\hat{V} = (1/2)(\alpha_1 + \alpha_2)[gN(t) + N_R(t)]\hat{\sigma}_0 + (\alpha_1 - \alpha_2)[gS_z(t) + S_{Rz}(t)]\hat{\sigma}_z$ is responsible for the blueshift experienced by polaritons as a result of polariton-polariton and polariton-exciton interactions. α_1 and α_2 are the constants of interaction of excitons with equal and opposite spins, respectively, and g defines the exciton fraction in the polariton state. $\hat{\sigma}_0$ and $\hat{\sigma}_{x,y,z}$ are the 2×2 identity matrix and the Pauli matrices, respectively. $N(t)$ and $N_R(t)$ are the occupations of the polariton condensate and the reservoir of incoherent excitons. $S_z(t)$ and $S_{Rz}(t)$ describe the imbalance in populations of spin-up and spin-down components of the polariton condensate and the exciton reservoir, respectively. The operator $\hat{R} = (1/2)(R_s + R_o)N_R(t)\hat{\sigma}_0 + (R_s - R_o)S_{Rz}(t)\hat{\sigma}_z$ describes the incoming flow from the exciton reservoir to the polariton condensate. R_s and R_o are the same- and opposite-spin scattering rates from the spin-

polarized reservoir to the condensate. Γ is the polariton decay rate. In our model, we explicitly account for the stochasticity of formation and evolution of a polariton condensate under a time-modulated pump. Namely, in addition to the random initial conditions we take into account quantum fluctuations experienced by the order parameter. The stochastic fluctuations described by the last term in Eq. (1) are described as a spin-resolved complex white noise $\hat{D}|\eta(t)\rangle$, for which the following correlators apply: $\langle\eta(t)|\hat{\sigma}_x|\eta(t')\rangle = 0$ and $\langle\eta(t)|\eta(t')\rangle = \delta(t-t')$ [18,25]. The noise amplitude is determined by the balance between gain and losses in the polariton condensate: $\hat{D}^2 \propto (\hat{R} - \Gamma\hat{\sigma}_0)$.

The evolution of the reservoir of incoherent excitons described by the spinor $|N_R\rangle = [N_{R+}(t), N_{R-}(t)]^T$ obeys the following rate equation:

$$d_t|N_R\rangle = |P\rangle - (\Gamma_X\hat{\sigma}_0 + \hat{W})|N_R\rangle + \Gamma_S(\hat{\sigma}_x - \hat{\sigma}_0)|N_R\rangle, \quad (2)$$

where Γ_X is the decay rate of excitons, Γ_S is the spin-relaxation rate in the reservoir. The operator $\hat{W}$ describing the outflow from the reservoir can be obtained from $\hat{R}$ by replacing $N_R(t) \rightarrow N(t)$ and $S_{Rz}(t) \rightarrow S_z(t)$. $|P\rangle = P(t)|p\rangle$ describes the nonresonant pumping of the exciton reservoir. $P(t)$ is the shape of the pulse, $|p\rangle = (p_+, p_-)^T$ is responsible for the circular polarization degree of the pump.

In the model, we take into account the effect of temperature on the gain and relaxation processes as well as on the stochastic processes [26–29]:

$$R_{s,o}(T) = R_{s,o}^{(0)}[1 - R_T T \exp(-\delta E/k_B T)], \quad (3a)$$

$$\Gamma_{X,S}(T) = \Gamma_{X,S}^{(0)} + \gamma_T T, \quad (3b)$$

where $\delta E = E_X - E_0$ is the splitting between the exciton and polariton energies, $R_{s,o}^{(0)}$ and $\Gamma_{X,S}^{(0)}$ are the values of the corresponding rates at zero temperature, R_T and γ_T are parameters of the model.

The simulation of the power dependence of the polarization statistics of the condensates demonstrates a good qualitative agreement with the experiment (see lower panel in Fig. 2). In the simulation, the laser pump power is related to the model parameter P as $\sim(P/P_{th})^\zeta$, where ζ is a dimensionless damping factor for the optical excitation which provides the best fit at $\zeta = 0.55$ (see Ref. [30] for other parameters). It incorporates the effects of the pump power and temperature of the experiment on the share of energy transferred from the optical pump to the sample as well as the spatial overlap of the exciton reservoir and the polariton condensate. The pump power increase leads to the increase of the noise term in Eq. (1). The enhanced noise is responsible for the collapse of the circular polarization degree of the condensate shown in Figs. 2(c) and 2(d). Our theory also reproduces well the experimental distribution of spin polarization with temperature (lower panel in

Fig. 3). One can see that the widths of the distributions increase with temperature likewise in the experiment and theory.

Both temperature and pump power increase affect the noise term in Eq. (1) according to Eqs. (3). The randomness of spin in each realization is captured well by our simulations [Fig. 4(b)]. We see that the probability of a subsequent realization of a fully spin polarized condensate n times in a row exhibits a nearly exponential decrease with the increase of n. Furthermore, the slope of this dependence in a logarithmic scale is essentially the same in the simulation and experiment. The above characteristics together with the possibility of generating regularly spaced realizations at high repetition rate set out the key requirements for true random number generation (RNG). The ability to control the polarization distribution bias by pump ellipticity and high temperature operation present further practical advantages.

We note that the present model predicts the quenching of two peaks in the distribution function of the condensate polarization at about 130 K, in agreement with the experimental data. At 130 K the magnitude of noise in Eq. (1) becomes so large that the polarized states of the seed of the condensate do not survive to form a condensate with a steady polarization. This critical temperature is governed by an interplay of the buildup of a polarized condensate provided by the stimulated scattering process and the depolarization of the condensate caused by the noise. In order to shift the critical temperature up one would need to reduce the noise. This can be achieved, potentially, by further reduction of the overlap of the condensate and the reservoir as well as choosing optimal exciton-cavity mode detunings not accessible in the present sample at high temperatures.

We note that none of the previous polarization studies on single-shot polariton condensates (Refs. [31–34]) have shown a bistable behavior as demonstrated here. In previous untrapped polariton condensates, the polarization has been either pinned or spread randomly throughout the whole Poincare sphere. The crucial difference here is the optical trapping of the condensate which helps in two ways: (i) the condensate is near the ground state ($k = 0$), where TE-TM splitting is small enough for a strong spin polarization [16], and (ii) the reservoir noise is reduced due to the small overlap with the condensate [35].

Indeed polarization chaos has been observed in other driven dissipative nonlinear systems [36,37]. However, the crucial difference with previous studies is that the combination of the strong coupling regime with the high finesse of the microcavity allows for spatial separation of the pump and lasing regions resulting in strong suppression of the noise, critical for observation of spin bifurcations. Furthermore, the present study employs nonresonant excitation where the phase and polarization of the fluid are not imposed by the laser itself [38]. See Supplemental Material [39] for comparison of polarization features observed in trapped polaritonic systems such as ours with other nonlinear systems; the Supplemental Material is supported by Refs. [40–42].

In conclusion, we demonstrate stochastic spin dynamics of exciton-polariton condensates emerging under nonresonant optical pumping in the pulsed regime. The spontaneous symmetry breaking of polariton condensates under the linearly polarized single-shot pump is maintained up to the 130 K. We demonstrate the nearly perfect independence of the realizations of the spin-polarized polariton condensates at elevated temperatures due to the pump's relatively long pulse separation in time (≈ 13 ns) compared to the exciton lifetime (≈ 1 ns). The exciton lifetime may limit the system's operating speed to the gigahertz range. However, the ability to generate large lattices of condensates [43] to parallelize such RNGs could potentially yield data throughput in the order of hundreds of Gbps, demonstrating the potential for using this polariton system as a fast true RNG device.

---

*balas@materials.uoc.gr
†p.savvidis@westlake.edu.cn

[1] J. J. Hopfield and D. W. Tank, Science **233**, 625 (1986).

[2] S. Kirkpatrick, C. D. Gelatt, and M. P. Vecchi, Science **220**, 671 (1983).

[3] J. D. Bryngelson and P. G. Wolynes, Proc. Natl. Acad. Sci. U.S.A. **84**, 7524 (1987).

[4] J. P. Bouchaud, J. Stat. Phys. **151**, 567 (2013).

[5] D. Hung-Thu, *Frustrated Spin Systems*, 2nd revised ed. (World Scientific, Singapore, 2013).

[6] I. Bloch, J. Dalibard, and W. Zwerger, Rev. Mod. Phys. **80**, 885 (2008).

[7] M. J. Hartmann, J. Opt. **18**, 104005 (2016).

[8] J. Q. You and F. Nori, Nature (London) **474**, 589 (2011).

[9] T. Inagaki, K. Inaba, R. Hamerly, K. Inoue, Y. Yamamoto, and H. Takesue, Nat. Photonics **10**, 415 (2016).

[10] N. G. Berloff, M. Silva, K. Kalinin, A. Askitopoulos, J. D. Töpfer, P. Cilibrizzi, W. Langbein, and P. G. Lagoudakis, Nat. Mater. **16**, 1120 (2017).

[11] X. Xu, Y. Hu, Z. Zhang, and Z. Liang, Phys. Rev. B **96**, 144511 (2017).

[12] H. Ohadi, A. Dreismann, Y. G. Rubo, F. Pinsker, Y. del Valle-Inclan Redondo, S. I. Tsintzos, Z. Hatzopoulos, P. G. Savvidis, and J. J. Baumberg, Phys. Rev. X **5**, 031002 (2015).

[13] H. Ohadi, Y. del Valle-Inclan Redondo, A. Dreismann, Y. G. Rubo, F. Pinsker, S. I. Tsintzos, Z. Hatzopoulos, P. G. Savvidis, and J. J. Baumberg, Phys. Rev. Lett. **116**, 106403 (2016).

[14] H. Ohadi, A. J. Ramsay, H. Sigurdsson, Y. del Valle-Inclan Redondo, S. I. Tsintzos, Z. Hatzopoulos, T. C. H. Liew, I. A. Shelykh, Y. G. Rubo, P. G. Savvidis, and J. J. Baumberg, Phys. Rev. Lett. **119**, 067401 (2017).

[15] A. Kavokin, J. J. Baumberg, G. Malpuech, and F. P. Laussy, *Microcavities* (2017).

[16] A. Dreismann, H. Ohadi, Y. V. I. Redondo, R. Balili, Y. Rubo, S. I. Tsintzos, G. Deligeorgis, Z. Hatzopoulos, P. G. Savvidis, and J. J. Baumberg, Nat. Mater. **15**, 1074 (2016).

[17] H. Sigurdsson, A. J. Ramsay, H. Ohadi, Y. G. Rubo, T. C. H. Liew, J. J. Baumberg, and I. A. Shelykh, Phys. Rev. B **96**, 155403 (2017).

[18] I. I. Ryzhov, V. O. Kozlov, N. S. Kuznetsov, I. Yu. Chestnov, A. V. Kavokin, A. Tzimis, Z. Hatzopoulos, P. G. Savvidis, G. G. Kozlov, and V. S. Zapasskii, Phys. Rev. Research **2**, 022064(R) (2020).

[19] A. Askitopoulos, A. V. Nalitov, E. S. Sedov, L. Pickup, E. D. Cherotchenko, Z. Hatzopoulos, P. G. Savvidis, A. V. Kavokin, and P. G. Lagoudakis, Phys. Rev. B **97**, 235303 (2018).

[20] V. A. Lukoshkin, V. K. Kalevich, M. M. Afanasiev, K. V. Kavokin, Z. Hatzopoulos, P. G. Savvidis, E. S. Sedov, and A. V. Kavokin, Phys. Rev. B **97**, 195149 (2018).

[21] E. Sedov, V. Lukoshkin, V. Kalevich, Z. Hatzopoulos, P. G. Savvidis, and A. Kavokin, ACS Photonics **7**, 1163 (2020).

[22] E. S. Sedov, V. A. Lukoshkin, V. K. Kalevich, P. G. Savvidis, and A. V. Kavokin, Phys. Rev. Research **3**, 013072 (2021).

[23] S. I. Tsintzos, A. Tzimis, G. Stavrinidis, A. Trifonov, Z. Hatzopoulos, J. J. Baumberg, H. Ohadi, and P. G. Savvidis, Phys. Rev. Lett. **121**, 037401 (2018).

[24] Y. del Valle-Inclan Redondo, H. Ohadi, Y. G. Rubo, O. Beer, A. J. Ramsay, S. I. Tsintzos, Z. Hatzopoulos, P. G. Savvidis, and J. J. Baumberg, New J. Phys. **20**, 075008 (2018).

[25] M. Wouters, I. Carusotto, and C. Ciuti, Phys. Rev. B **77**, 115340 (2008).

[26] L. Schultheis, A. Honold, J. Kuhl, K. Köhler, and C. W. Tu, Phys. Rev. B **34**, 9027 (1986).

[27] D. D. Solnyshkov and H. Terças, K. Dini, and G. Malpuech, Phys. Rev. A **89**, 033626 (2014).

[28] F. Bassani, F. Tassone, and L. C. Andreani, Excitons and polaritons in quantum wells, in *Semiconductor Superlattices and Interfaces*, edited by A. Stella and L. Miglio (Elsevier, New York, 1993), p. 187.

[29] Y. Yamamoto, F. Tassone, and H. Cao, *Semiconductor Cavity Quantum Electrodynamics*, Springer Tracts in Modern Physics (Springer, New York, 2000).

[30] The polariton-exciton energy splitting is $\delta E = 25$ meV. The exciton and polariton decay rates and the spin-relaxation rate in the reservoir are $\Gamma_X^{(0)} = \Gamma_S^{(0)} = 0.04$ ps^{-1} and $\Gamma = (g-1)\Gamma_C + g\Gamma_X$, where $\Gamma_C = 0.1$ ps^{-1} is the cavity photon decay rate. The exciton fraction in the polariton state is $g = 0.5$. The energy and linewidth splitting in linear polarizations are $\hbar\Delta = -30$ μeV, $\gamma = 0.2\Delta$. The stimulated scattering rates are $R_s^{(0)} = 0.005$ ps^{-1} and $R_o^{(0)} = 0.8R_s$. The interaction constants are $\hbar\alpha_1 = 10\,\mu$eV and $\alpha_2 = -0.5\alpha_1$.

[31] J. J. Baumberg, A. V. Kavokin, S. Christopoulos, A. J. D. Grundy, R. Butté, G. Christmann, D. D. Solnyshkov, G. Malpuech, G. Baldassarri Höger von Högersthal, E. Feltin, J. F. Carlin, and N. Grandjean, Phys. Rev. Lett. **101**, 136409 (2008).

[32] H. Ohadi, E. Kammann, T. C. H. Liew, K. G. Lagoudakis, A. V. Kavokin, and P. G. Lagoudakis, Phys. Rev. Lett. **109**, 016404 (2012).

[33] V. G. Sala, F. Marsault, M. Wouters, E. Galopin, I. Sagnes, A. Lemaître, J. Bloch, and A. Amo, Phys. Rev. B **93**, 115313 (2016).

[34] M. V. Kochiev, V. V. Belykh, N. N. Sibeldin, C. Schneider, and S. Höfling, Phys. Rev. B **99**, 035310 (2019).

[35] K. Orfanakis, A. F. Tzortzakakis, D. Petrosyan, P. G. Savvidis, and H. Ohadi, Phys. Rev. B **103**, 235313 (2021).

[36] M. Virte, K. Panajotov, H. Thienpont, and M. Sciamanna, Nat. Photonics **7**, 60 (2013).

[37] T. R. Raddo, K. Panajotov, B.-H. V. Borges, and M. Virte, Sci. Rep. **7**, 14032 (2017).

[38] L. Dominici, D. Colas, A. Gianfrate, A. Rahmani, V. Ardizzone, D. Ballarini, M. De Giorgi, G. Gigli, F. P. Laussy, D. Sanvitto, and N. Voronova, Phys. Rev. Research **3**, 013007 (2021).

[39] See Supplemental Material at http://link.aps.org/supplemental/10.1103/PhysRevLett.128.117401 for a comparison of polarization features observed in trapped polaritonic systems such as ours with other nonlinear systems.

[40] M. San Miguel, Q. Feng, and J. V. Moloney, Phys. Rev. A **52**, 1728 (1995).

[41] J. Kasprzak, R. André, L. S. Dang, I. A. Shelykh, A. V. Kavokin, Y. G. Rubo, K. V. Kavokin, and G. Malpuech, Phys. Rev. B **75**, 045326 (2007).

[42] D. Read, T. C. H. Liew, Y. G. Rubo, and A. V. Kavokin, Phys. Rev. B **80**, 195309 (2009).

[43] H. Ohadi, Y. del Valle-Inclan Redondo, A. J. Ramsay, Z. Hatzopoulos, T. C. H. Liew, P. R. Eastham, P. G. Savvidis, and J. J. Baumberg, Phys. Rev. B **97**, 195109 (2018).